Published in final edited form as:

Cancer Discov. 2020 December ; 10(12): 1894–1911. doi:10.1158/2159-8290.CD-19-0970.

The folate cycle enzyme MTHFR is a critical regulator of cell response to MYC-targeting therapies.

Angela Su[#,1], **Frank Ling**[#,1], **Camille Vaganay**[1], **Gaetano Sodaro**[1], **Chaïma Benaksas**[1], **Reinaldo Dal Bello**[1], **Antoine Forget**[1], **Bryann Pardieu**[1], **Kevin H. Lin**[2], **Justine C. Rutter**[2], **Christopher F. Bassil**[2], **Gael Fortin**[1], **Justine Pasanisi**[1], **Iléana Antony-Debré**[3], **Gabriela Alexe**[4,5], **Jean-François Benoist**[6], **Alain Pruvost**[7], **Yana Pikman**[4,8], **Jun Qi**[5,8], **Marie-Hélène Schlageter**[9,10], **Jean-Baptiste Micol**[3,11], **Giovanni Roti**[12], **Thomas Cluzeau**[13], **Hervé Dombret**[14], **Claude Preudhomme**[15], **Nina Fenouille**[1], **Lina Benajiba**[1,16], **Hava M. Golan**[17], **Kimberly Stegmaier**[4,5], **Camille Lobry**[&,3], **Kris C. Wood**[&,2], **Raphael Itzykson**[&,1], **Alexandre Puissant**[&,1]

[1]INSERM UMR 944, IRSL, St Louis Hospital, University of Paris, Paris, France

[2]Department of Pharmacology and Cancer Biology, Duke University, Durham, NC, USA

[3]INSERM UMR 1287, Gustave Roussy Institute, Université Paris-Saclay, Villejuif, France

[4]Department of Pediatric Oncology, Dana-Farber Cancer Institute and Boston Children's Hospital, Harvard Medical School, Boston, MA, USA

[5]The Broad Institute of Harvard University and Massachusetts Institute of Technology, Cambridge, MA, USA

[6]AP-HP, Biochemistry-Hormonology Department, Robert Debré Hospital, Paris, France

[7]Paris-Saclay University, CEA, INRAE, Département Médicaments et technologies pour la santé, SPI, Gif-sur-Yvette, France

[8]Department of Cancer Biology, Dana-Farber Cancer Institute and Boston Children's Hospital, Harvard Medical School, Boston, MA, USA

[9]AP-HP, Cellular Biology Department, St Louis Hospital, Paris, France

[10]INSERM U 1131, IRSL, St Louis Hospital, University of Paris, Paris, France

[11]Department of Hematology, Gustave Roussy Institute, Villejuif, France

[12]University of Parma, Department of Medicine and Surgery, Parma, Italy

[13]Department of Hematology, Centre Hospitalier Universitaire, Nice, France

[14]LTL, IRSL, St Louis Hospital, Paris, France

[15]Laboratory of Hematology, CHU Lille, Lille, France

Corresponding authors: Alexandre Puissant, Raphael Itzykson, INSERM U944 | CNRS UMR 7212, St Louis Hospital, 16 rue de la grange aux belles, 75010 PARIS, FRANCE, Phone number: +33 1 53 72 40 63, alexandre.puissant@inserm.fr, raphael.itzykson@aphp.fr.

[#]These authors contributed equally to this work.

[&]These senior authors contributed equally to this work.

[16]AP-HP, Hematology Department, St Louis Hospital, Paris, France

[17]Zlotowski Center for Neuroscience, Ben-Gurion University of the Negev, Beer-Sheva, Israel

Abstract

Deciphering the impact of metabolic intervention on response to anticancer therapy may elucidate a path toward improved clinical responses. Here, we identify amino acid-related pathways connected to the folate cycle whose activation predicts sensitivity to MYC-targeting therapies in acute myeloid leukemia (AML). We establish that folate restriction and deficiency of the rate-limiting folate cycle enzyme, MTHFR — which exhibits reduced-function polymorphisms in about 10% of Caucasians — induce resistance to MYC targeting by BET and CDK7 inhibitors in cell lines, primary patient samples, and syngeneic mouse models of AML. Further, this effect is abrogated by supplementation with the MTHFR enzymatic product, CH_3-THF. Mechanistically, folate cycle disturbance reduces H3K27/K9 histone methylation and activates a *SPI1* transcriptional program counteracting the effect of BET inhibition. Our data provide a rationale for screening *MTHFR* polymorphisms and the folate cycle status to nominate patients most likely to benefit from MYC-targeting therapies.

INTRODUCTION

The rewiring of cellular metabolic activities represents a major determinant of cancer progression and is considered a hallmark of cancer (1). Metabolic reprogramming supports the acquisition and maintenance of malignant properties. The integration of high-throughput *omics* technologies like metabolomics and loss-of-function screening has revolutionized our understanding of how metabolic dependencies support cancer cell proliferation (2–4). Although non-proliferating cell activity depends primarily on catabolic demands, proliferating cells must balance the divergent catabolic and anabolic requirements of sustaining cellular homeostasis while duplicating mass, and thus become dependent on a plethora of metabolic pathways not typically essential for normal tissue maintenance (5). This peculiar metabolic rewiring of neoplastic cells engenders metabolic liabilities that can be exploited to design innovative therapeutic strategies, notably to increase the therapeutic index of existing anticancer therapies. For instance, it was recently observed that dietary supplementation of histidine enhances leukemic cell sensitivity to the widely used chemotherapeutic agent, methotrexate, an antimetabolite which inhibits *de novo* nucleotide synthesis (6). This suggests that dietary supplementation can be leveraged to curtail the toxicity of anticancer therapies while maximizing on-target activity.

In addition to diet-mediated enhancement of antimetabolite-based chemotherapy, metabolic perturbation may substantially influence response to therapies targeting oncogenes involved in hijacking of neoplastic cell metabolism. In that regard, *MYC* represents a paradigmatic oncogene as this transcription factor is deregulated in over 50% of human cancers and reprograms many aspects of cell metabolism including glucose uptake and glycolysis, glutaminolysis, serine/glycine metabolism, and lipid biosynthesis (7). A general feature of MYC deregulation is its transcriptional regulation by super-enhancer genomic regions. These clusters of enhancers are densely occupied by transcription factors and chromatin

regulators — including BET bromodomain proteins, and CDK7 and CDK9 kinases — and have been exploited over the past decade as essential targets owing to their MYC transcriptional regulator function. Therefore, indirect targeting of MYC transcription through inhibition of these essential regulators has shown great promise in pre-clinical studies, notably in AMLs harboring MLL gene fusions (8). Inhibitors targeting these chromatin remodelers are currently in phase 1–2 clinical trials in advanced solid tumors and hematologic malignancies (8–10).

The diverse metabolic alterations induced by MYC may constitute another source of unique metabolic rewiring that could be exploited to nominate new treatment strategies. These approaches may enhance cell susceptibility to its inhibition by this new class of inhibitors or enable identification of patient populations most likely to benefit from MYC-targeting therapies. Here, we present a roadmap for the identification of metabolic predictors of resistance to diverse chromatin-remodeling drugs in cancers. We integrate *omic* profiling, and shRNA- and CRISPR/Cas9-based functional approaches to identify and delineate mechanisms by which metabolism perturbation impacts response to MYC-targeting therapies.

RESULTS

Folate Restriction Promotes Resistance to Therapies Targeting MYC Expression.

BET proteins interact with acetylated histones in active regulatory domains (promoters and enhancers) and promote RNA PolII activity. Despite the general nature of this mechanism, BET inhibitors show selective effects on gene expression through suppression of *MYC* and MYC-related transcriptional programs (8, 11, 12). Two AML patient cohorts (TCGA-LAML, n=198 and GSE14468, n=526) were queried with multiple gene sets related to MYC transcriptional programs as well as vitamin, amino acid, and nucleotide metabolism using single sample Gene Set Enrichment Analysis (ssGSEA). Correlation between gene sets was queried across all patients from each cohort to pinpoint potential crosstalk between active MYC programs and specific metabolic pathways (Figure 1A, Table S1). Whereas many pathways related to nucleotide (pyrimidine, purine), tetrahydrofolate salvage, lysine, cysteine/methionine, arginine/proline alanine/aspartate/glutamate and valine/leucine/isoleucine metabolism were strongly correlated with active MYC signatures, those associated with folate cycle and biosynthesis, histidine, glycine/serine/threonine, beta-alanine, phenylalanine/tyrosine, and tryptophan metabolism were all poorly correlated with active MYC signatures, suggesting that these pathways are not regulated by MYC, and thus may be hijacked by cancer cells to undergo metabolic rewiring and escape from drug-induced MYC inhibition (Figure 1B). To investigate this, three AML cell lines (KG1a, IMS-M2, and U937) were grown in media deprived of amino acids or vitamins belonging to the metabolic pathways poorly correlated with active MYC signatures and were then treated with BET inhibitor OTX015 (13) (Figure 1C). Although phenylalanine and histidine starvation increased resistance to OTX015 in a subset of AML cell lines, folic acid starvation consistently enhanced resistance to OTX015 in all cell lines tested.

To investigate further the relationship between folic acid starvation and increased BET inhibitor resistance, we compiled a panel of AML cell lines harboring diverse genetic

alterations. Supporting our previous observation, folic acid-starved media significantly increased the area under curve (AUC) and half-maximal inhibitory concentration (IC_{50}) of OTX015 versus standard media (Figure 1D). The effect of folic acid removal was also evaluated in cell lines treated either with a second BET inhibitor, JQ1, or with THZ-1, a covalent CDK7 inhibitor, another key factor in transcriptional elongation at super-enhancer regions and a strong inhibitor of MYC expression (14) (Figure 1E and S1). In both conditions, folic acid withdrawal significantly dampened AML cell line sensitivity to JQ1 and THZ-1. Previous studies have focused on the role of a specific BET family member, BRD4, which is potently inhibited by JQ1 and OTX015 and serves as one of the main targets triggering their deleterious effects. Therefore, we studied selective suppression of *BRD4* by short hairpin RNA (shRNA) in two AML cell lines. As seen with JQ1 and OTX015 treatments, there was a striking viability decrease upon *BRD4* knockdown, which was significantly attenuated with folic acid starvation (Figure 1F). To further characterize the phenotypic consequences of folic acid withdrawal on the sensitivity of AML cells to OTX015, we performed colony formation assays and established that a 125-fold decrease in folic acid concentration (from 1 mg/L to 0.008 mg/L in standard versus conditioned media, respectively) significantly increased U937 cell colony formation in the presence of OTX015 (Figure 1G). This was accompanied by a decrease in OTX015-induced apoptosis (Figure 1H). Moreover, folic acid withdrawal markedly increased the IC_{50} of OTX015 in a cohort of *MLL*-translocated primary patient samples with AML (Figure 1I).

To control for bias of *in vitro* culture conditions on the increased BET inhibitor resistance induced by folate starvation, mice injected with *MLL-AF9*-driven AML cells were fed with regular or no folic acid diet before JQ1 treatment. Intracellular folic acid concentrations approximated 56 ng/mL/10^6 cells irrespective of whether extracellular folic acid levels were physiological (63 ng/mL in mouse serum) or supra-physiological (1000 ng/mL in standard media, Table S2). From 40 ng/mL folic acid to complete folic acid withdrawal in the culture media, we observed a similar 2.5-fold reduction in intracellular folic acid as in leukemic blasts harvested from mice fed with no folic acid diet. Folic acid levels in mouse serum, liver, and red blood cells were significantly decreased in animals fed for two, four, and eight weeks with the folic acid-restricted compared to those fed with a regular diet (Figure S2A). This was associated with increased homocysteine levels (hyperhomocysteinemia) in plasma versus those fed with regular diet, confirming that folate starvation recapitulated physiological features reported in previous studies (15, 16) (Figure 1J). Over eight weeks, folate withdrawal did not cause a significant drop in hematocrit, white blood cell count, or weight (Figure S2B). Consistent with our *in vitro* results, the anti-leukemic activity of JQ1 was markedly attenuated in animals fed no folate diet versus those fed regular diet (Figure 1K). This was associated with a significant decrease in the overall survival of folic acid-restricted mice treated with JQ1 in comparison with their regular diet-fed counterparts (Figure S3).

Depletion of the Folate-Cycle Rate-Limiting Enzyme, MTHFR, Enhances Resistance to BET Inhibitors.

Dietary folic acid undergoes several conversion steps into intermediate metabolites before generation of 5,10-methylene-THF (5,10-CH_2 THF). 5,10-CH_2 THF is then either reduced

in the folate cycle or oxidized in the formate-producing tetrahydrofolate salvage cycle, per cellular needs. Despite the fact that folic acid can be processed through these two interconnected pathways, we observed in our previous ssGSEA analyses that active MYC gene signatures were highly correlated with activation of tetrahydrofolate salvage cycle, but not folate cycle-related gene sets (Figures 1A and 1B). This implies some negative regulatory relationship between MYC and the folate cycle, prompting us to investigate further the consequences of the suppression of each enzyme of the folate cycle on the sensitivity to OTX015. Five central enzymes control the multi-step conversion of dietary folate into 5,10-methylene-THF (5,10-CH_2 THF) before its reduction to 5-methyl-THF (5-CH_3 THF) and recycling to THF (Figure 2A). We infected IMS-M2 AML cells with two hairpins that markedly reduced their expression levels (Figure 2B). Although hairpins targeting serine hydroxymethyltransferase *1* (SHMT1) and 5-methyltetrahydrofolate-homocysteine methyltransferase (MTR) did not markedly alter OTX015 response, those targeting the two dihydrofolate reductase isoenzymes (DHFR and DHFR2) as well as 5,10-methylenetetrahydroflate reductase (MTHFR) which expectedly reduced the THF/Folate and 5-CH_3 THF/THF ratios, respectively, substantially increased the OTX015 IC_{50} by averages of 3- and 7-fold, respectively (Figure 2C, S4A, and S4B). Based on these observations, the combination of OTX015 with the DHFR inhibitor, methotretrexate, was antagonistic at a wide range of concentrations across four AML cell lines, OCI-AML2, KG1a, U937, and IMS-M2 (Figure S5).

Given that MTHFR is the rate-limiting folate cycle enzyme and that its knockdown induced the most striking decrease in OTX015 sensitivity in IMS-M2 cells, we pursued our investigation of the effect of the two *MTHFR*-directed shRNAs on OTX015 response by interrogating the same AML cell lines (Figures 2D–2F) and confirmed that MTHFR suppression substantially weakened the response of all tested cell lines to increasing doses of OTX015 (Figure 2E). The folate cycle is intimately interconnected to the methionine cycle through which it regulates methionine and homocysteine levels. Given the interdependence of both cycles, we investigated whether alteration of the methionine cycle could affect OTX015 response in AML cells as consistently as alteration of the folate cycle. We modulated the expression of S-methyl-5'-thioadenosine phosphorylase (MTAP), a critical enzyme involved in methionine salvage, in IMS-M2 and U937 AML cell lines, using two *MTAP*-directed shRNAs exhibiting different knockdown effectiveness on MTAP expression (Figure S6A). Although OTX015 resistance was enhanced by MTAP suppression in both cell lines, more sustained MTAP knockdown was required to decrease OTX015 sensitivity in U937 cells (Figure S6B). Given that MYC can control anti-apoptotic programs, we also explored whether MTHFR suppression antagonized inhibition of the anti-apoptotic protein, BCL-2, by venetoclax. MTHFR knockdown did not affect viability response nor cytochrome c release in two AML cell lines tested (Figures S7A and S7B).

Finally, we abrogated Mthfr expression in primary murine MLL-AF9-driven AML cells using two *Mthfr*-directed shRNAs before treatment of engrafted mice with JQ1 (Figures 2G–2I). In animals transplanted with *Mthfr*-depleted blasts, leukemic burden was not significantly decreased by JQ1 treatment compared to control counterparts which exhibited striking sensitivity to JQ1 (Figure 2H). Thus, the overall survival of mice injected with *Mthfr*-depleted cells was significantly shorter than mice with control leukemic cells after

JQ1 treatment (Figure 2I). Similarly, *Mthfr* knockdown significantly reduced the anti-leukemic effect of JQ1 in an additional AML mouse model driven by the *Cbfb-MYH11* fusion oncogene (Figure S8). Collectively, these data nominated MTHFR as a critical folate cycle enzyme whose impairment increases resistance to MYC-targeting therapies.

Frequent Polymorphisms in Human Populations Associated with Reduced MTHFR Activity Promote Resistance to BET Inhibitors.

Previous studies have extensively characterized two common *MTHFR* genetic variants, *C677T* and *A1298C*, encoding MTHFR enzyme variants with reduced activity, resulting in hyperhomocysteinemia in humans. In particular, homozygous variant 677 TT and 1298 CC genotypes are present in ~10% of Caucasians and display only 30% and 60% of the homozygous wild-type 677 CC and 1298 AA enzyme activities, respectively (17, 18). To explore the impact of these *MTHFR* variants on BET inhibitor resistance, we deployed CRISPR-Cas9-based genome editing in KG1a cells to introduce these two non-synonymous single nucleotide polymorphisms in *MTHFR*, thereby generating isogenic cell lines exhibiting all variant combinations. Five KG1a clones either 1) wild-type 677 CC and 1298 AA, 2) heterozygous 677 CT or 1298 AC, or 3) homozygous 677 TT or 1298 CC, were selected and genotyped via an allelic discrimination technique (Figure 3A). Although clones heterozygous for any of the two variants had similar sensitivity to OTX015 as wild-type clones, 677 TT and 1298 CC homozygous KG1a clones were significantly more resistant to OTX015 than their wild-type counterpart (Figure 3B). Furthermore, colony numbers from 677 TT and 1298 CC homozygous KG1a clones were substantially higher than those of wild-type KG1a clones upon OTX015 treatment (Figure 3C). Based on these results, we divided a cohort of 16 *MLL*-translocated primary AML patient cells into two subgroups by *MTHFR* genotype: wild-type and single-heterozygous versus homozygous and compound heterozygous for any of two *MTHFR* variants (Table S3). Patients displaying homozygous or compound heterozygous *MTHFR* genotypes for any of the two variants responded significantly less to OTX015 than those with wild-type homozygous and heterozygous *MTHFR* genotypes (Figure 3D). Using the same criteria of patient subclassification based on *MTHFR* variant status, we observed the same significant trend of OTX015 response in a second cohort of Core Binding Factor (CBF) AML patients (Figure S9A, Table S4). Finally, we engineered a tractable *MLL-AF9*-driven mouse model of AML in which *Mthfr* genotype status was either homozygous wild-type, heterozygous or homozygous knockout. We established that loss of a single *Mthfr* copy, which phenocopies in mice a partial impairment in MTHFR activity caused by non-synonymous single nucleotide polymorphisms on *MTHFR* (19), was sufficient to decrease overall leukemia burden and, most importantly, attenuate JQ1 sensitivity in *MLL-AF9*-driven leukemias (Figure 3E).

Because MTHFR impairment promotes BET inhibitor resistance, we hypothesized that wild-type MTHFR overexpression may conversely enhance sensitivity of AML cells lacking proper MTHFR function due to the presence of the two genetic *C677T* and *A1298C* *MTHFR* variants. Exogenous DD-tagged wild-type *MTHFR* was overexpressed in AML cells exhibiting various 677 CC and 1298 AA genotypes (Figure 3F). This markedly increased OTX015 sensitivity of AML cell lines displaying homozygous and compound heterozygous *MTHFR* genotypes for any of the two variants in comparison with cell lines

exhibiting either a wild-type or heterozygous 677 CT genotype (Figure 3G). A similar analysis performed on the isogenic *MTHFR*-edited KG1a clones showed that those displaying homozygous 677 TT or 1298 CC genotypes were significantly more sensitized to OTX015 upon overexpression of wild-type *MTHFR* than their homozygous wild-type 677 CC and 1298 AA counterparts (Figure 3H). We then reasoned that supplementation with the end-product metabolite synthesized by MTHFR, 5-CH_3 THF, may induce a similar effect on OTX015 response as wild-type *MTHFR* overexpression. Despite the increased IMS-M2 and U937 cell line resistance to OTX015 in response to MTHFR depletion, we thus observed that treatment with exogenous 5-CH_3 THF restored a cytotoxic effect of OTX015 similar to that observed in shCT-infected cells (Figure 3I). Consistent with this observation, exogenous 5-CH_3 THF substantially enhanced response to OTX015 of homozygous 677 TT or 1298 CC *MTHFR* KG1a clones compared to their wild-type *MTHFR* counterparts (Figure 3J). In addition, exogenous 5-CH_3 THF sensitized primary patient cells exhibiting an altered *MTHFR* genotype to OTX015 (Figure 3K). We finally asked whether the 5-CH_3 THF supplementation could improve sensitivity in all individuals or only in those who are folate deficient by treating wild-type, heterozygous or homozygous *Mthfr* knockout MLL-AF9-driven cells with increasing concentrations of 5-CH_3 THF (Figure S9B). While the sensitivity to OTX015 of wild-type Mthfr cells was not affected by a wide range of 5-CH_3 THF concentrations, a 4-fold increase in 5-CH_3 THF levels (from approximately 3 to 12 μg/mL) was required to sensitize cells whose Mthfr expression was decreased from 50% to 100%, respectively, to OTX015.

Disruption of Folate Cycle Activity Increases Intracellular Levels of the Methyltransferase Inhibitor S-adenosylhomocysteine, and Impairs H3K27 and H3K9 Methyltransferase Activities.

We next used metabolism profiling to characterize the effect of folate pathway alteration on global cell metabolism in U937 cells. Steady state levels of 113 metabolites highly enriched in pathways either directly coupled to the folate cycle such as pyrimidine metabolism as well as histidine, glycine/serine/threonine, and cysteine/methionine/taurine/glutathione metabolism, or indirectly associated with folate metabolism including urea cycle-related pathways such as arginine/proline, alanine, aspartate, glutamate, and beta-alanine metabolism, were significantly changed by folate starvation (Figure 4A, S10A and Table S5). Interestingly, this revealed a significant increase in S-adenosylhomocysteine (SAH), an intermediate in homocysteine synthesis from all methylation reactions involving the methionine-derived metabolite, S-adenosylmethionine (SAM), as a methyl donor. ShRNA-mediated *MTHFR* depletion induced a similar increase in SAH levels as that observed upon folate withdrawal in AML cell lines U937 and IMS-M2 (Figure 4B). This was associated with a reduction in SAM production and SAM/SAH ratio (Figure S10B and S10C). Finally, SAH supplementation increased OTX015 IC_{50} by a magnitude similar to that measured upon folate starvation in KG1a and U937 cells (Figure 4C). Of note, depleting methionine in media of IMS-M2 cells (by 300-fold in methionine low “L” condition) enhanced the cytoprotective effect of SAH against OTX015 to a similar extent as that induced by folic acid starvation. In U937 and KG1a cells, this caused even greater resistance to OTX015 than folate restriction alone. Together, these data suggest that increased intracellular SAH is critical in mediating OTX015 resistance in response to impaired folate cycle activity.

SAH is a potent inhibitor of SAM-dependent methylation reactions (20). We thus hypothesized that increased SAH induced by folate cycle suppression may directly impact methylation on histone H3. Methylation profiling on H3 histone marks revealed that FA starvation significantly decreased dimethylation (me2) and trimethylation (me3) of H3K9 and H3K27, respectively (Figure 4D). Furthermore, MTHFR impairment reduced H3K27me3 and H3K9me2 in human and murine AML cells (Figures 4E–4G). This decreased methylation status resulted from a significant drop in H3K27 and H3K9 methyltransferase activity upon folate starvation or MTHFR depletion (Figure 4H).

To identify precisely the class of H3K27 and H3K9 methyltransferases whose decreased activity affects sensitivity to BET inhibitors, we deployed a CRISPR/Cas9 screening strategy using a dedicated library targeting 325 epigenetic regulators including DNA writers and erasers such as histone methylases/demethylases to search for depletion or enrichment of specific guides under a single JQ1 concentration (Table S6). sgRNA library-transduced cells were treated with JQ1 or DMSO and sampled weekly for 2 weeks of treatment to determine the composition of the sgRNA pools by deep sequencing. We identified a core component of the H3K27-methyltransferase PRC2 complex, *EED*, and two other SET-domain-containing H3K9 methyltransferases, *EHMT1* and *SETDB1*, as top rescuer hits whose knockout rescued cells from JQ1 (Figure 4I and Table S7). Conversely, guides targeting three H3K9 demethylase enzymes, *KDM1A*, *KDM3B*, and *JMJD1C* were relatively depleted in the presence of JQ1 versus control, suggesting that their loss sensitized cells to JQ1. To confirm this, two hairpins that reduced EED, EHMT1, and SETDB1 protein levels were transduced in U937 cells and markedly alleviated OTX015 sensitivity, phenocopying the cytoprotective effect of MTHFR depletion previously observed in BET inhibitor-treated cells (Figure 4J and Figure S11A). Besides the critical function of EED in scaffolding the PRC2 complex, another subunit (EZH2, which can be directly targeted by small-molecule inhibitors such as EPZ-6438) triggers the catalytic methyltransferase activity of PRC2. OTX015 treatment in combination with EPZ-6438 was antagonistic at a wide range of concentrations in three AML cell lines, consistent with the identification of H3K9 and H3K27 methyltransferases, either alone or in complex, as critical mediators of response to BET inhibitors (Figure S11B).

Folate Cycle Disruption Activates a SPI1 Transcriptional Program in Response to BET Inhibition.

Our data imply that folate cycle suppression reduces H3K27 and H3K9 methylation. This suggests that folate cycle disruption may induce transcriptomic and epigenetic rewiring of AML cells to activate a specific transcriptional program which mitigates BET inhibitor efficacy. We profiled the transcriptomes of two AML cell lines, IMS-M2 and U937, treated with OTX015 for 24 hours with or without folic acid, using RNA sequencing (RNAseq). Consistent with the fact that folate withdrawal decreases methylation of repressive H3K27me3 and H3K9me2 histone marks, we observed a global increase in gene expression, despite OTX015 treatment, which has been shown to preferentially repress genes marked by super-enhancers (412 and 706 significantly upregulated versus 160 and 520 significantly downregulated genes in IMS-M2 and U937 cells, respectively, Figure S12A). Accordingly, we identified 75 and 15 genes significantly upregulated and downregulated between both

folate-deprived cell lines, respectively, compared to cells in regular media with OTX015 (Figure 5A). An open-ended enrichment analysis was conducted comparing gene expression variations i) between DMSO and OTX015 conditions irrespective of folate status and ii) upon folate withdrawal irrespective of DMSO or OTX015 treatment. Genesets were considered as significantly enriched based on the cut-offs p value ≤ 0.05 and false discovery rate (FDR) ≤ 0.25 on the entire set of signatures from the c2, c3, and c6 (MsigDB) and ENCODE and CHEA collections (Figure 5B). Consistent with the reported effect of BET inhibitors on MYC expression, we established that, irrespective of folate status, gene sets related to MYC transcriptional program were highly enriched (FDR < 0.25) in genes whose expression is suppressed by OTX015 in the cell lines tested (Figure 5B, **top panel**). Conversely, many gene sets related to SPI1 transcriptional program and interferon signaling and regulatory factors (IRF), a well-reported SPI1-connected pathway (21, 22), were drastically enriched in genes whose expression is enhanced by folate withdrawal specifically with OTX015 treatment (Figure 5B, **bottom panel**). To investigate whether OTX015-induced activation of SPI1-related transcriptional programs reflects epigenetic changes induced by folate starvation, we profiled genome-wide distribution of H3K27me3 and H3K9me2 by chromatin immunoprecipitation (ChIP) sequencing of OTX015-treated IMS-M2 and U937 cells with regular or folate-restricted media. This confirmed that H3K27me3 binding signal in a 10Kb-region flanking gene transcriptional starting sites (TSS) was decreased with folic acid starvation (Figure S12B). A total of 3868 and 4214 genes were annotated within the 50kb-flanking H3K27me3 or H3K9me2-marked regions exhibiting a decreased methylation level with folate withdrawal in OTX015-treated IMS-M2 and U937 cells, respectively (Figure 5C). By overlapping these gene sets with genes identified by RNAseq as upregulated with folate starvation (530 and 1140 genes in IMS-M2 and U937 cells, respectively), we narrowed down the list of genes whose upregulation was directly associated with H3K27me3 and H3K9me2 demethylation to 93 and 202 genes in IMS-M2 and U937 cells, respectively. These two gene lists were then queried by overlapping analysis with two ENCODE and CHEA datasets generated from curated target genes of transcription factors defined based on published ChIP-chip, ChIP-seq, and other transcription factor binding-site profiling studies (Figure 5D). Two gene signatures related to SPI1 target genes from ENCODE and CHEA scored among the top enriched pathways, confirming that SPI1 transcriptional program activation in response to OTX015 treatment and folate withdrawal results from H3K27 and H3K9 demethylation. Finally, using the top genes from SPI1 target-related gene sets which were upregulated upon folate withdrawal and OTX015 treatment, we designed a SPI1 consensus transcriptional target mini signature. We used qRT-PCR to assess alteration of these signature genes and confirmed induction of these SPI1 target genes in response to MTHFR depletion and OTX015 treatment (Figure 5E). Similar induction was observed in 677 TT and 1298 AA *MTHFR* homozygous KG1a clones in comparison with their wild-type counterpart (Figure 5F).

To explore functionally whether SPI1 transcriptional program activation induced by folate cycle disruption promotes resistance to BRD4 inhibition, we knocked down SPI1 in IMS-M2 and U937 cells before folate withdrawal or MTHFR suppression (Figures 5G and 5H). SPI1 depletion significantly reduced OTX015 resistance in AML cells whose folate cycle activity was disturbed or MTHFR expression was suppressed (Figures 5I and 5J). In

addition, SPI1 depletion alleviated resistance to JQ1 of MLL-AF9 blasts injected in mice fed with folic acid-restricted diet (Figure S13). Similarly, Spi1 knockdown abrogated resistance to OTX015 of MLL-AF9-transformed *Mthfr* knockout primary murine cells both *in vitro* and *in vivo* (Figure 5K and 5L). Together, these data suggest that folate cycle disruption promotes H3K27 and H3K9 demethylation, which activates a SPI1 transcriptional program capable of promoting resistance to BRD4 inhibition.

DISCUSSION

Here we revealed folate-connected metabolic gene signatures whose activation was poorly correlated with an active MYC transcriptional program in AML. This core metabolic network is composed of the histidine, serine, threonine and glycine pathways, which serve as inputs to the folate cycle (23), the beta-alanine/histidine synthesis pathway (24), and the phenylalanine- and DHFR-dependent tetrahydrobiopterin regeneration pathway (25). We also identified the tryptophan pathway as part of this core metabolic unit, likely because this pathway produces vitamin B6, an essential co-factor for synthesis of 5-CH_3 THF from serine and THF (26).

Folate metabolism supports manifold transformations dependent on THF oxidative state, with 5,10-CH_2-THF, 5-CH_3-THF, and 10-CHO-THF each supporting distinct biosynthetic functions. 5,10-CH_2-THF is used in three ways: 1) by serine hydroxymethyltransferase (SHMT1) or thymidylate synthase (TYMS) to synthesize serine or sustain *de novo* thymidylate synthesis, respectively; 2) by MTHFR for reduction to 5-CH_3-THF and entrance into the folate cycle, which stimulates the methylation cycle; or, 3) by oxidation into 10-CHO-THF to sustain the THF salvage pathway which promotes purine synthesis and maintains mitochondrial redox homeostasis (23). Although a subset of folate- and MTHFR-related gene sets were poorly correlated with MYC signatures, we demonstrate that gene sets related to the THF salvage pathway and purine synthesis were strongly associated with active MYC gene signatures. This is consistent with previous studies showing that MYC promotes expression of *SHMT2*, *MTHFD2*, and *MTHFD1L* mitochondrial enzymes which contribute to purine production through the THF salvage pathway (27, 28). Despite the fact that both the folate cycle and tetrahydrofolate salvage pathways are interconnected within folate metabolism, our data hereby suggest that these pathways can be uncoupled on the basis of their connectivity to MYC transcriptional programs.

Consistent with this observation, we demonstrate functionally that folate starvation promotes resistance to MYC targeting by either BRD4 or CDK7 inhibitors, or *BRD4*-directed shRNAs. Previous studies suggest that folate cycle, *de novo* thymidylate synthesis, and THF salvage pathways compete for a limiting pool of 5,10-CH_2-THF upon folate starvation. For instance, thymidylate synthesis is preserved in folate deficiency at the expense of the methylation cycle, which relies on activity of 5,10-CH_2-THF-dependent MTHFR from the folate cycle. This favorable balance toward sustained thymidylate synthesis results from the activity of a critical cytosolic 10-CHO-THF-producer, MTHFD1, which translocates to the nucleus upon folate starvation to maintain *de novo* thymidylate biosynthesis (29, 30). Moreover, nuclear MTHFD1 also regulates transcription by direct binding to BRD4-occupied chromatin (31). These observations suggest that all folate-related metabolic

pathways are not affected to the same extent by folate restriction. Although some pathways (10-CHO-THF-dependent reactions) persist without folate due to the plasticity of enzymes such as MTHFD1, the folate cycle and its associated methylation cycle are more severely impaired and thereby influence cell response to BET inhibitors.

We pinpoint MTHFR as the most critical folate-related mediator of resistance to BRD4 inhibitors and demonstrate that the presence of either of two *MTHFR* polymorphisms (677C>T; 1298A>C) in a homozygous state predicts sensitivity to BET inhibition. We observe that folate cycle disturbance in AML cells results in intracellular accumulation of SAH, the downstream effector of MTHFR knockdown triggering BET inhibitor resistance. Because the conversion of SAH to homocysteine is reversible but SAH-preferential, our results are consistent with the fact that hyperhomocysteinemia is accompanied by an elevation of SAH in *Mthfr* knockout animals (19, 32). Given that SAH is a potent inhibitor of SAM-dependent methylation, folate cycle impairment suppresses H3K27 and H3K9 methyltransferases and targets methylation across the whole genome of AML cells. We validated that a SAM-dependent H3K27-methyltransferase PRC2 complex member, EED, scored among three downstream mediators of resistance to BET inhibitors, thereby recapitulating that suppression of the PRC2 complex promotes BET inhibitor resistance in AML (33).

Decreased H3K27 and H3K9 methylation upon folate cycle alteration combined with BET inhibition activates SPI1 and IRF/Interferon signaling transcriptional programs. These programs are tightly linked through physical interactions between SPI1 and IRF4 or IRF8 in hematopoietic stem and progenitor cells (34, 35). We establish that SPI1 program activation is the main downstream effector of resistance to BET inhibitors with folate or MTHFR deficiency. Indeed, inhibition of demethylase KDM1A increases resistance to BRD4 inhibition via an IRF8/SPI1-mediated epigenetic rewiring (36). This supports the idea that the folate cycle dynamically influences epigenetic AML cell resistance by favoring an adaptive transcriptional plasticity relying on widespread, SPI1-dependent transcriptional changes. The latter acts as a compensatory mechanism to sustain cell survival despite BRD4 inhibition, a canonical epigenetic regulator of enhancer regions.

Two clinical trials are currently evaluating the clinical efficacy of combining BET inhibitors and Azacitidine, the standard-of-care treatment of elderly AML patients (NCT02303782 and NCT02543879), thereby raising clinical interest in identifying relevant biomarkers of response to BET inhibitors. Although no significant prevalence of the two *MTHFR C677T* and *A1298C* variants was described in AML, their frequencies were found significantly increased in therapy-related AML patients who contracted breast cancer as primary disease or who were previously treated with cyclophosphamide-based anti-cancer therapies (37). This suggests that the metabolic consequences of altered MTHFR activity could trigger resistance to a wide collection of chemotherapeutic agents beyond just those known to target the folate cycle, or could even participate in therapy-induced leukemogenesis. Beside folate and MTHFR deficiencies, deficits in folate cycle enzyme cofactors like cobalamin (vitamin B12) or pyridoxal phosphate (from vitamin B6) also affect methylation and cause hyperhomocysteinemia (38, 39). Up to 38% of older adults exhibit a food-cobalamin malabsorption syndrome characterized by B12 deficiency while the incidence of B6

deficiency in European institutionalized elderly people reaches up to 75%. Thus, our study likely underestimates the prevalence of folate cycle deficiency-induced BET inhibitor resistance among AML patients, who are mainly elderly. Additional work is required to evaluate to what extent the effect of folate/methylation cycle disruption upon B12 and B6 deficiencies or loss-of-function mutations in enzymes controlling these metabolic pathways may, like MTHFR insufficiency, promote resistance to MYC-targeting therapies.

Our study supports that MTHFR and folate cycle deficiencies remodel the epigenetic landscape to shape transcriptional plasticity which represents a mechanism of resistance to epigenetic therapies. Their status should be carefully assessed by measurements of total plasma homocysteine or CH_3-THF levels when enrolling patients with hematological diseases in clinical trials of BET inhibitors. Dietary supplementation with CH_3-THF may thereby represent a relatively low-risk intervention that might allow for a greater clinical benefit to curtail transcriptional adaptation of malignant cells to MYC-targeting therapies.

MATERIAL AND METHODS

Cell Culture

U937 and KG1a cell lines were purchased from the American Type Culture Collection and OCI-AML2 cell line was purchased from DSMZ. MOLM-13 was provided by Dr. Benjamin Ebert; IMS-M2 by Pr. Hervé Dombret; and MOLM-14 cell lines by Dr. Scott Armstrong (Dana-Farber Cancer Institute, Boston, MA, USA). Identity of all cell lines was confirmed by STR loci profiling. All cell lines were tested negative for mycoplasma using MycoAlertTM PLUS Mycoplasma Detection Kit (#LT07–705, Lonza). All cell lines, except MOLM-13 and Kasumi-3, were maintained in RPMI 1640 (Invitrogen) supplemented with 1% penicillin-streptomycin and 10% fetal bovine serum (FBS, Sigma-Aldrich) at 37 °C with 5% CO_2. MOLM-13 cells were maintained in RPMI 1640 supplemented with 1% penicillin-streptomycin and 20% FBS. Kasumi-3 cells were maintained in RPMI 1640 supplemented with 1% penicillin/streptomycin and 10% FBS with 20 ng per ml GM-CSF (Peprotech). The 293T cells were maintained in Dulbecco’s modified Eagle’s medium (Invitrogen) supplemented with 10% FBS (Sigma-Aldrich) and 100 units per ml penicillin/streptomycin (Invitrogen).

Primary patient AML blasts were collected from bone marrow aspirates or peripheral blood samples after obtaining patient written informed consent under Saint-Louis Hospital and Lille University Hospital Internal Review Board-approved protocols. These studies were conducted in accordance with recognized ethical guidelines from the Declaration of Helsinki and were approved by an institutional review board. Mononuclear cells isolated using Ficoll-Paque Plus (Amersham Biosciences) were thawed before drug treatment. These cells were maintained in RPMI 1640 medium supplemented with 20% FBS, 20 ng/ml IL-3 (#200–03, Peprotech), 20 ng/ml IL-6, 20 ng/ml GM-CSF (#300–03, Peprotech), 10 ng/nl G-CSF (#300–23, Peprotech), 10 ng/ml EPO (#100–64, Peprotech), 50 ng/ml TPO (#300–18, Peprotech), 100 ng/ml FLT3-Ligand (#300–19, Peprotech) and 100 ng/ml SCF (#300–07, Peprotech).

For folate starvation experiments, cell lines were washed twice in PBS, and maintained for 18 hours in no folic acid RPMI 1640 medium (Invitrogen, #27016–021) supplemented with 10% dialyzed FBS (Sigma-Aldrich, #F0392) and 100 units per ml penicillin/streptomycin (Invitrogen) prior to treatment with drugs or infection with shRNAs. Primary patient cells were kept in the same medium as cell lines supplemented with the same concentration of cytokines as previously stated. The corresponding + folic acid RPMI 1640 medium was generated using no folic acid RPMI 1640 medium supplemented with 1mg/L folic acid (Sigma-Aldrich-Aldrich, #F8758).

For functional characterization of the effect of single amino acid starvation on cell response to BET inhibitors, cell lines were washed twice in PBS, and maintained for 18 hours in no folate and no amino acid RPMI 1640 medium (Genaxxon Bioscience) supplemented with all amino acids and folic acid at the exception of the amino acid to test, 10% dialyzed FBS, and 100 units per ml penicillin/streptomycin prior to treatment with BET inhibitors.

Metabolomic Analyses

To determine relative levels of intracellular metabolites, extracts were prepared and analyzed by LC/MS/MS. 16 hours before extraction, 15×10^6 U937 cells were plated in quadruplicate in folic acid-free RPMI 1640 supplemented with 10% dialyzed FBS and 100 units/ml penicillin/streptomycin +/− 1mg/L folic acid. Metabolites were extracted on dry ice with 4 mL of 80% methanol (−80°C), as described previously (40). Insoluble material was pelleted by centrifugation at 3000*g* for 5 min, followed by two subsequent extractions of the insoluble pellet with 0.5 ml of 80% methanol, with centrifugation at 16000*g* for 5 min. The 5 ml metabolite extract from the pooled supernatants was dried down under nitrogen gas using an N-EVAP (Organomation Associates, Inc).

Dried pellets were re-suspended using 20 μL HPLC grade water for mass spectrometry. 10 μl were injected and analyzed using a 5500 QTRAP triple quadrupole mass spectrometer (AB/SCIEX) coupled to a Prominence UFLC HPLC system (Shimadzu) via selected reaction monitoring (SRM) of a total of 547 endogenous water soluble metabolites for steady-state analyses of samples. Some metabolites were targeted in both positive and negative ion mode for a total of 391 SRM transitions using pos/neg polarity switching. ESI voltage was +4900V in positive ion mode and −4500V in negative ion mode. The dwell time was 3 ms per SRM transition and the total cycle time was 1.55 seconds. Approximately 10–14 data points were acquired per detected metabolite. Samples were delivered to the MS via normal phase chromatography using a 4.6 mm i.d × 10 cm Amide Xbridge HILIC column (Waters Corp.) at 350 μL/min. Gradients were run starting from 85% buffer B (HPLC grade acetonitrile) to 42% B from 0–5 minutes; 42% B to 0% B from 5–16 minutes; 0% B was held from 16–24 minutes; 0% B to 85% B from 24–25 minutes; 85% B was held for 7 minutes to re-equilibrate the column. Buffer A was comprised of 20 mM ammonium hydroxide/20 mM ammonium acetate (pH=9.0) in 95:5 water:acetonitrile. Peak areas from the total ion current for each metabolite SRM transition were integrated using MultiQuant v2.0 software (AB/SCIEX). A Student's t-test was performed to assess significance of pairwise comparisons. All data are $\log_2$-transformed and normalized against the average control condition. No or small variations in metabolite production compared to average

control condition appears closest to the white color on the heatmap. Decreased or increased metabolite production compared to the average control condition is represented by a gradient of color from blue to red respectively. The MetaboAnalyst software (www.metaboanalyst.ca) was used to perform pathway enrichment analysis on the set of top metabolites hits identified by steady-state profiling. No specific manual settings were needed to analyze the list of metabolites.

Pooled CRISPR/Cas9 Epigenetic Screen

OCI-AML2 cells were seeded into six-well plates at a density of 3×10^6 cells per well and transduced at MOI 0.2. 24 hours post-transduction, cells were replated into puromycin-containing media. A sample was collected at 48 hours post-puromycin to confirm library coverage in the transduced population. Transduced cells were expanded in puromycin for 10 days before drug, when the transduced population was split into vehicle (DMSO) and JQ1 conditions and maintained for two weeks. Deep sequencing was performed by Hudson Alpha Institute for Biotechnology on an Illumina Nextseq platform (75 bp, single-ended) to identify differences in library composition. Determinations of genetic essentiality and drug sensitization/resistance were made by evaluating differential guide compositions between the initial population and subsequent drug-treated and vehicle-treated cells populations. Briefly, the fractional representation (FR) for a guide within a sample was normalized to the sum of all guides attributed to that sample. A direct comparison between two samples entailed the quotient of the respective FRs, which we term the depletion metric (DM). The five guide-level DMs for each gene were then collapsed to gene-level scores by taking the average. Guides which totaled fewer than 200 counts for a given sample were excluded from analysis. Genetic essentiality was calculated by considering the depletion/enrichment of the vehicle-treated population over time (DMSOfinal / initial). Drug sensitization/resistance was calculated by considering the depletion/enrichment of the drug-treated population relative to the vehicle-treated population ($Drug_{final}$ / $DMSO_{final}$). All depletion/enrichment effects are reported as $\log_2$ ratios. All described manipulations were performed in R. Additional information is provided in the supplementary material and methods section.

CRISPR/Cas9-Mediated Introduction of Single Nucleotide Polymorphisms On MTHFR

Top and bottom sgRNAs targeting the C677 and A1298 *MTHFR* sites (Top_C677: 5’-CACCGAAGCTGCGTGATGATGAAAT-3’ and Bottom_C677: 5’-AAACATTTCATCATCACGCAGCTTC-3’; Top_A1298: 5’-CACCGTTCAAAGACACTTTCTTCAC-3’ and Bottom_A1298: 5’-AAACGTGAAGAAAGTGTCTTTGAAC-3’) were annealed and phosphorylated as previously described (24157548), and ligated into the BbSSI-digested pSpCas9(BB)-2A-GFP (PX458) vector (Addgene, # 48138) to generate PX458_sgC677 and PX458_sgA1298 constructs. 1×10^6 KG-1a cells were washed in PBS before resuspension in 100 μl Opti-MEM medium (ThermoFisher Scientific, # 31985–047). 10 μg PX458_sgC677 or PX458_sgA1298 vector and 0.3 μM SSODN_C677 (5’-TGGCAGGTTACCCCAAAGGCCACCCCGAAGCAGGGAGCTTTGAGGCTGACCTGAAGCACTTGAAGGAGAAGGTGTCTGCGGGAGTCGATTTCATCATCACGCAGCTTTTCTTTGAGGCTGACACA-3’) or SSODN_A1298 (5’-TTGGGGAGCTGAAGGACTACTACCTCTTCTACCTGAAGAGCAAGTCCCCCAAGGA

GGAGCTGCTGAAGATGTGGGGGGAGGAGCTGACAAGTGAAGCAAGTGTCTTTGAAGTCTTCGTTCTTTAC-3') were added into the mix of Opti-MEM and cells to generate isogenic KG-1a clones expressing either *MTHFR* 677 C>T, A1298 A>C, or wild-type genetic variant, respectively.

Cells were then electroporated using a NEPA21 eletroporator (Nepagene) following a poring pulse of 150V, length: 5 ms, interval: 50 ms, No: 2, D. rate: 10% and polarity: +, and a transfer pulse of 20V, length: 50 ms, interval: 50 ms, No: 5, D. rate: 40% and polarity: +/−. Electroporated cells were then incubated for 48 hours in presence of 10 μM SCR7 (Selleckchem, # S7742) prior to single cell sorting into 96-well plates. Clones were then grown and *MTHFR* genetic status was screened by allelic discrimination assay.

Integrated ChIP- and RNA-sequencing analysis.

SICER-identified significantly decreased H3K9me2 (14651 regions in IMS-M2; 4842 regions in U937) and H3K27me3 (4048 regions in IMS-M2; 4855 regions in U937) peaks in OTX−FA versus OTX+FA conditions were annotated for the 2 nearest genes using GREAT (41) within a 50kb window upstream and downstream. The union of lists of annotated genes per cell line was kept defining a list of all genes in the vicinity of lost H3K9me2 or H3K27me3 (3961 genes for IMSM2; 4416 genes for U937).

Significantly upregulated genes (fold change > 1.2; p-value < 0.05) identified by RNA-seq experiments comparing OTX−FA versus OTX+FA conditions were selected (623 genes in IMS-M2; 1342 genes in U937) compared to the lists of genes proximal to decreased H3K9me2 and H3K27me3 regions identified previously leading to an overlap of 93 genes in IMS-M2 and 202 genes in U937. Additional information is provided in the supplementary material and methods section. ChIP-seq and RNA-seq data are available at GEO database under accession code GSE152442.

In silico tests for Pearson correlation calculation between MYC-related and metabolic gene sets

Single-sample GSEA (ssGSEA) was used to calculate separate enrichment scores for each pairing of a sample whose transcriptomic data was available from TCGA-LAML (42) or GSE14468 (43) and a given gene set (queried from MSigDB for MYC and KEGG-related gene signatures or manually curated from BIOCYC for other metabolic gene sets). A Pearson correlation matrix was computed between each ssGSEA score for the core MYC signature and all gene sets of interest obtained across all patients from a given cohort. Connected metabolic pathways were clustered based on the median of Pearson correlation scores obtained from each individual pathway.

In Vivo Transplantation

The French National Committee on Animal Care reviewed and approved all mouse experiments. Sample size was influenced by historical penetrance and consistency of MLL-AF9-driven *in vivo* models. For the *Mthfr* knockout AML mouse model, BALB/cJ mice were purchased from Charles River Laboratories. Each recipient mouse was transplanted with transduced $Sca1^{-}$/c-Kit^{+} myeloid progenitors sorted from the total bone marrow of

three donor mice. Approximatively two months post-transplantation, sick mice were euthanized and bone marrow harvested before flow-based sorting of MLL-AF9-positive granulo-monocytic bone marrow progenitor population (GFP^+/Sca-1^-/c-Kit^+/$Cd16/32^+$/$Cd34^+$) and PCR-based confirmation of *Mthfr* knockout status. 0.2×10^6 MLL-AF9-positive $Mthfr^{+/+}$, $Mthfr^{+/-}$, and $Mthfr^{-/-}$ cells were then reinjected into sublethally-irradiated secondary recipient mice treated daily by intraperitoneal injection with 50mg/kg JQ1 (10% DMSO + 90% G5W).

For folate starvation experiments, 5-week old male C57BL/6J mice were given regular or folate-deficient casein-reconstituted diet (U8958 Version 0262, Safe-Diets) for 4 weeks before sublethal irradiation (350cGy) and injection with 0.2×10^6 MLL-AF9-positive L-GMP cells before treatment with 35mg/kg or 50mg/kg JQ1 (10% DMSO + 90% G5W) for 7 days. For *Mthfr* knockdown experiments, MLL-AF9-positive L-GMP cells were infected with a control or two *Mthfr*-directed shRNAs cloned into an MSCV-miRE-SV40-eBFP vector modified from the MSCV-miRE_shBRD9_561-SV40-GFP vector (Addgene, # 75139) by substitution of the GFP cassette with an eBFP fluorescent marker. 0.2×10^6 infected cells were injected into sublethally-irradiated 5-week old C57BL/6J recipient mice. Additional information is provided in the supplementary material and methods section.

Statistical Analysis

Statistical analysis was done using Microsoft Excel, Prism 5.03 (GraphPad) or indicated software for more dedicated analysis. Statistical significance was determined by unpaired Student's t-test after testing for normal distribution. For samples with significantly different variances, Welch's correction was applied. Samples with non-normal distribution (with the assumption of no Gaussian distribution of the group) were analyzed using a nonparametric Mann-Whitney test, and the level of significance (alpha) was always set at 0.05. For comparison of three or more groups, nonparametric Kruskall-Wallis and Dunn's multiple comparisons tests were used, and the level of significance was always set at 0.05.

Data Availability

Transcriptomic data from primary patient samples with AML are available from TCGA-LAML (GDC Data Portal, National Cancer Institute) and from GEO database under accession numbers: GSE14468. U937 and IMS-M2 ChIP-seq and RNA-seq data are available at GEO database under accession code GSE152442.

Supplementary Material

Refer to Web version on PubMed Central for supplementary material.

ACKNOWLEGMENTS

We are indebted to Jean-Michel Cayuela, Carole Albuquerque, Christophe Roumier and Céline Decroocq from the Saint-Louis and Lille Tumor Banks for primary patient samples; Veronique Montcuquet, Nicolas Setterblad, Christelle Doliger, and Sophie Duchez from the Saint-Louis Research Institute Core Facility; and the technical staff from the DBA (Diagnostic Biologique Automatisé) platform of Saint-Louis Hospital. We are grateful to Dr. Lucio H. Castilla for providing us with the *Cbfb-MYH11* knock-in mouse model. This work was supported by the ATIP/AVENIR French research program (to A.P.), the EHA research grant for Non-Clinical Advanced Fellow (to A.P.), the Ligue Nationale Contre le Cancer (to A.P.), the Mairie de Paris Emergences grants (to A.P.), the INCA PLBIO

program (PLBIO20-246, to A.P.), the Fondation Gustave Roussy (to C.L.), and NIH 5R35 CA210030 (to K.S.). This work was also supported by grants from Oncoethix, S.A. (now Merck), Association Laurette Fugain (ALF2014-10), and Gilead International Research Scholarship in Onco-haematology to R.I. A.P. is a recipient of support from the ERC Starting program (758848) and supported by the St Louis Association for leukemia research.

CONFLICTS OF INTEREST

K.S. has previously consulted for Rigel Pharmaceuticals and receives grant funding from Novartis on topics unrelated to this manuscript.

REFERENCES

1. Hanahan D, Weinberg RA. Hallmarks of cancer: the next generation. Cell. 2011;144:646–74. [PubMed: 21376230]
2. Hsu PP, Sabatini DM. Cancer cell metabolism: Warburg and beyond. Cell. 2008;134:703–7. [PubMed: 18775299]
3. Lunt SY, Vander Heiden MG. Aerobic glycolysis: meeting the metabolic requirements of cell proliferation. Annual review of cell and developmental biology. 2011;27:441–64.
4. Pavlova NN, Thompson CB. The Emerging Hallmarks of Cancer Metabolism. Cell metabolism. 2016;23:27–47. [PubMed: 26771115]
5. Luengo A, Gui DY, Vander Heiden MG. Targeting Metabolism for Cancer Therapy. Cell chemical biology. 2017;24:1161–80. [PubMed: 28938091]
6. Kanarek N, Keys HR, Cantor JR, Lewis CA, Chan SH, Kunchok T, et al. Histidine catabolism is a major determinant of methotrexate sensitivity. Nature. 2018;559:632–6. [PubMed: 29995852]
7. Stine ZE, Walton ZE, Altman BJ, Hsieh AL, Dang CV. MYC, Metabolism, and Cancer. Cancer discovery. 2015;5:1024–39. [PubMed: 26382145]
8. Zuber J, Shi J, Wang E, Rappaport AR, Herrmann H, Sison EA, et al. RNAi screen identifies Brd4 as a therapeutic target in acute myeloid leukaemia. Nature. 2011;478:524–8. [PubMed: 21814200]
9. Chen H, Liu H, Qing G. Targeting oncogenic Myc as a strategy for cancer treatment. Signal transduction and targeted therapy. 2018;3:5. [PubMed: 29527331]
10. Puissant A, Frumm SM, Alexe G, Bassil CF, Qi J, Chanthery YH, et al. Targeting MYCN in neuroblastoma by BET bromodomain inhibition. Cancer discovery. 2013;3:308–23. [PubMed: 23430699]
11. Delmore JE, Issa GC, Lemieux ME, Rahl PB, Shi J, Jacobs HM, et al. BET bromodomain inhibition as a therapeutic strategy to target c-Myc. Cell. 2011;146:904–17. [PubMed: 21889194]
12. Filippakopoulos P, Qi J, Picaud S, Shen Y, Smith WB, Fedorov O, et al. Selective inhibition of BET bromodomains. Nature. 2010;468:1067–73. [PubMed: 20871596]
13. Boi M, Gaudio E, Bonetti P, Kwee I, Bernasconi E, Tarantelli C, et al. The BET Bromodomain Inhibitor OTX015 Affects Pathogenetic Pathways in Preclinical B-cell Tumor Models and Synergizes with Targeted Drugs. Clinical cancer research : an official journal of the American Association for Cancer Research. 2015;21:1628–38. [PubMed: 25623213]
14. Kwiatkowski N, Zhang T, Rahl PB, Abraham BJ, Reddy J, Ficarro SB, et al. Targeting transcription regulation in cancer with a covalent CDK7 inhibitor. Nature. 2014;511:616–20. [PubMed: 25043025]
15. Devlin AM, Arning E, Bottiglieri T, Faraci FM, Rozen R, Lentz SR. Effect of Mthfr genotype on diet-induced hyperhomocysteinemia and vascular function in mice. Blood. 2004;103:2624–9. [PubMed: 14630804]
16. Mikael LG, Pancer J, Jiang X, Wu Q, Caudill M, Rozen R. Low dietary folate and methylenetetrahydrofolate reductase deficiency may lead to pregnancy complications through modulation of ApoAI and IFN-gamma in spleen and placenta, and through reduction of methylation potential. Molecular nutrition & food research. 2013;57:661–70. [PubMed: 23112124]
17. Ranganathan P, McLeod HL. Methotrexate pharmacogenetics: the first step toward individualized therapy in rheumatoid arthritis. Arthritis and rheumatism. 2006;54:1366–77. [PubMed: 16645965]

18. Weisberg I, Tran P, Christensen B, Sibani S, Rozen R. A second genetic polymorphism in methylenetetrahydrofolate reductase (MTHFR) associated with decreased enzyme activity. Molecular genetics and metabolism. 1998;64:169–72. [PubMed: 9719624]
19. Chen Z, Karaplis AC, Ackerman SL, Pogribny IP, Melnyk S, Lussier-Cacan S, et al. Mice deficient in methylenetetrahydrofolate reductase exhibit hyperhomocysteinemia and decreased methylation capacity, with neuropathology and aortic lipid deposition. Human molecular genetics. 2001;10:433–43. [PubMed: 11181567]
20. Chen NC, Yang F, Capecci LM, Gu Z, Schafer AI, Durante W, et al. Regulation of homocysteine metabolism and methylation in human and mouse tissues. FASEB journal : official publication of the Federation of American Societies for Experimental Biology. 2010;24:2804–17. [PubMed: 20305127]
21. Kubosaki A, Lindgren G, Tagami M, Simon C, Tomaru Y, Miura H, et al. The combination of gene perturbation assay and ChIP-chip reveals functional direct target genes for IRF8 in THP-1 cells. Molecular immunology. 2010;47:2295–302. [PubMed: 20573402]
22. Will B, Vogler TO, Narayanagari S, Bartholdy B, Todorova TI, da Silva Ferreira M, et al. Minimal PU.1 reduction induces a preleukemic state and promotes development of acute myeloid leukemia. Nature medicine. 2015;21:1172–81.
23. Ducker GS, Rabinowitz JD. One-Carbon Metabolism in Health and Disease. Cell metabolism. 2017;25:27–42. [PubMed: 27641100]
24. Boldyrev AA, Aldini G, Derave W. Physiology and pathophysiology of carnosine. Physiological reviews. 2013;93:1803–45. [PubMed: 24137022]
25. Shi W, Meininger CJ, Haynes TE, Hatakeyama K, Wu G. Regulation of tetrahydrobiopterin synthesis and bioavailability in endothelial cells. Cell biochemistry and biophysics. 2004;41:415–34. [PubMed: 15509890]
26. Badawy AA. Kynurenine Pathway of Tryptophan Metabolism: Regulatory and Functional Aspects. International journal of tryptophan research : IJTR. 2017;10:1178646917691938. [PubMed: 28469468]
27. Nikiforov MA, Chandriani S, O'Connell B, Petrenko O, Kotenko I, Beavis A, et al. A functional screen for Myc-responsive genes reveals serine hydroxymethyltransferase, a major source of the one-carbon unit for cell metabolism. Molecular and cellular biology. 2002;22:5793–800. [PubMed: 12138190]
28. Ye J, Fan J, Venneti S, Wan YW, Pawel BR, Zhang J, et al. Serine catabolism regulates mitochondrial redox control during hypoxia. Cancer discovery. 2014;4:1406–17. [PubMed: 25186948]
29. Field MS, Kamynina E, Agunloye OC, Liebenthal RP, Lamarre SG, Brosnan ME, et al. Nuclear enrichment of folate cofactors and methylenetetrahydrofolate dehydrogenase 1 (MTHFD1) protect de novo thymidylate biosynthesis during folate deficiency. The Journal of biological chemistry. 2014;289:29642–50. [PubMed: 25213861]
30. Green JM, MacKenzie RE, Matthews RG. Substrate flux through methylenetetrahydrofolate dehydrogenase: predicted effects of the concentration of methylenetetrahydrofolate on its partitioning into pathways leading to nucleotide biosynthesis or methionine regeneration. Biochemistry. 1988;27:8014–22. [PubMed: 3266075]
31. Sdelci S, Rendeiro AF, Rathert P, You W, Lin JG, Ringler A, et al. MTHFD1 interaction with BRD4 links folate metabolism to transcriptional regulation. Nature genetics. 2019;51:990–8. [PubMed: 31133746]
32. Castro R, Rivera I, Struys EA, Jansen EE, Ravasco P, Camilo ME, et al. Increased homocysteine and S-adenosylhomocysteine concentrations and DNA hypomethylation in vascular disease. Clinical chemistry. 2003;49:1292–6. [PubMed: 12881445]
33. Rathert P, Roth M, Neumann T, Muerdter F, Roe JS, Muhar M, et al. Transcriptional plasticity promotes primary and acquired resistance to BET inhibition. Nature. 2015;525:543–7. [PubMed: 26367798]
34. Pang SH, Minnich M, Gangatirkar P, Zheng Z, Ebert A, Song G, et al. PU.1 cooperates with IRF4 and IRF8 to suppress pre-B-cell leukemia. Leukemia. 2016;30:1375–87. [PubMed: 26932576]

35. Pham TH, Minderjahn J, Schmidl C, Hoffmeister H, Schmidhofer S, Chen W, et al. Mechanisms of in vivo binding site selection of the hematopoietic master transcription factor PU.1. Nucleic acids research. 2013;41:6391–402. [PubMed: 23658224]

36. Bell CC, Fennell KA, Chan YC, Rambow F, Yeung MM, Vassiliadis D, et al. Targeting enhancer switching overcomes non-genetic drug resistance in acute myeloid leukaemia. Nature communications. 2019;10:2723.

37. Guillem VM, Collado M, Terol MJ, Calasanz MJ, Esteve J, Gonzalez M, et al. Role of MTHFR (677, 1298) haplotype in the risk of developing secondary leukemia after treatment of breast cancer and hematological malignancies. Leukemia. 2007;21:1413–22. [PubMed: 17476281]

38. Kjeldby IK, Fosnes GS, Ligaarden SC, Farup PG. Vitamin B6 deficiency and diseases in elderly people--a study in nursing homes. BMC geriatrics. 2013;13:13. [PubMed: 23394203]

39. Stover PJ. Vitamin B12 and older adults. Current opinion in clinical nutrition and metabolic care. 2010;13:24–7. [PubMed: 19904199]

40. Fenouille N, Bassil CF, Ben-Sahra I, Benajiba L, Alexe G, Ramos A, et al. The creatine kinase pathway is a metabolic vulnerability in EVI1-positive acute myeloid leukemia. Nature medicine. 2017;23:301–13.

41. McLean CY, Bristor D, Hiller M, Clarke SL, Schaar BT, Lowe CB, et al. GREAT improves functional interpretation of cis-regulatory regions. Nature biotechnology. 2010;28:495–501.

42. Cancer Genome Atlas Research N, Ley TJ, Miller C, Ding L, Raphael BJ, Mungall AJ, et al. Genomic and epigenomic landscapes of adult de novo acute myeloid leukemia. The New England journal of medicine. 2013;368:2059–74. [PubMed: 23634996]

43. Wouters BJ, Lowenberg B, Erpelinck-Verschueren CA, van Putten WL, Valk PJ, Delwel R. Double CEBPA mutations, but not single CEBPA mutations, define a subgroup of acute myeloid leukemia with a distinctive gene expression profile that is uniquely associated with a favorable outcome. Blood. 2009;113:3088–91. [PubMed: 19171880]

SIGNIFICANCE

Although MYC-targeting therapies represent a promising strategy for cancer treatment, evidence of predictors of sensitivity to these agents is limited. We pinpoint that folate cycle disturbance and frequent polymorphisms associated with reduced MTHFR activity promote resistance to BET inhibitors. CH_3-THF supplementation thus represents a low-risk intervention to enhance their effects.

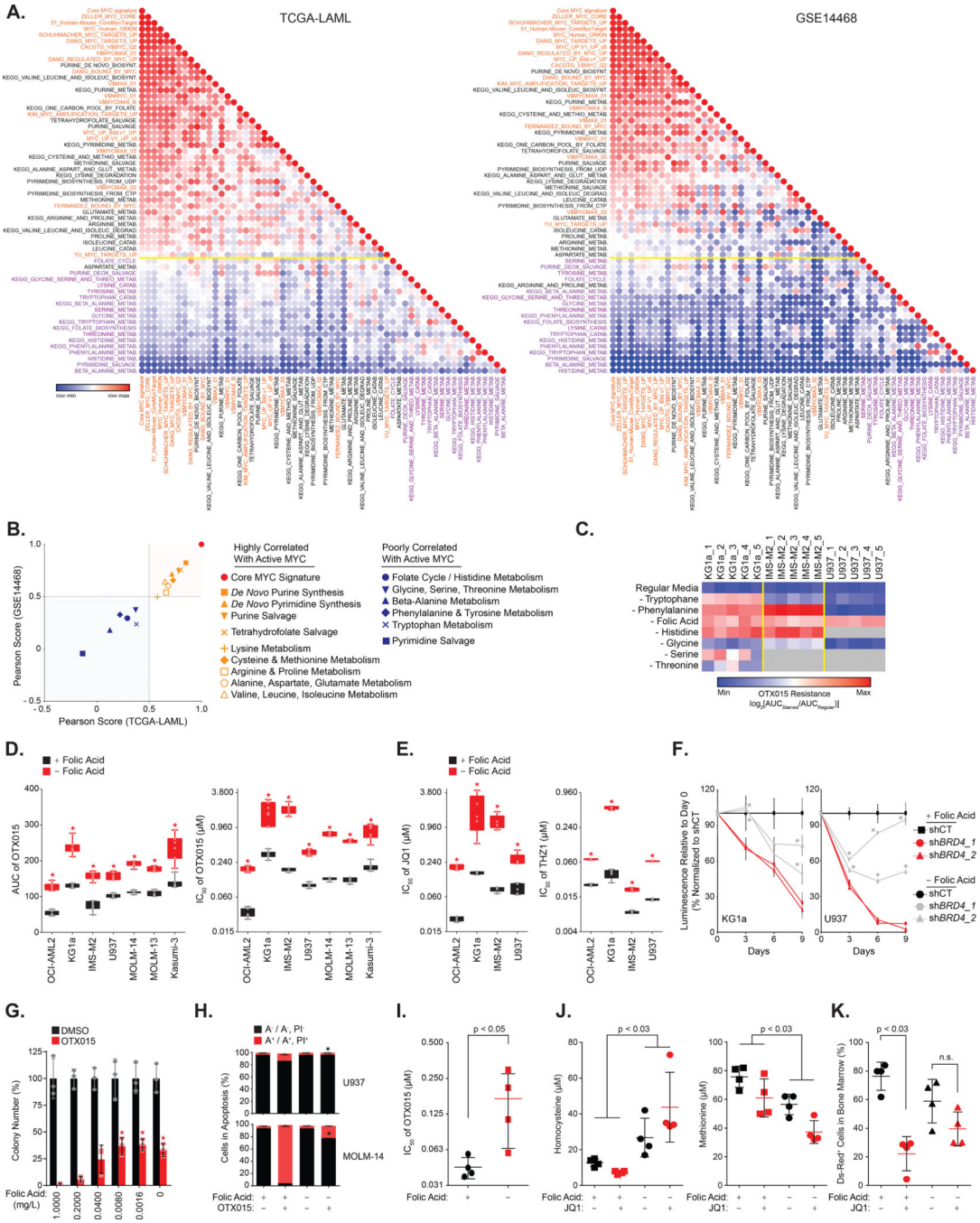

Figure 1: Folate restriction promotes resistance to MYC-targeting therapies.

(A) Heatmaps depicting Pearson correlation of MYC-related and metabolic gene sets (from KEGG and curated BIOCYC databases) interrogated using ssGSEA in two AML patient cohorts: TCGA-LAML; GSE14468. Orange connotes MYC-related gene sets; black and purple connote metabolic pathways most and least correlated with MYC-related signatures. Core MYC signature is defined by leading-edge genes from each MYC-related gene set.

(B) XY graph representation of two patient datasets (TCGA-LAML; GSE14468) by Pearson correlation of defined clusters of metabolic pathways with core MYC signature. Red

indicates core transcriptional MYC signature; orange and blue indicate metabolic signatures clusters highly and poorly correlated with core MYC signature.

(C) Heatmap of OTX015 resistance of three AML cell lines (KG1a, IMS-M2, U937) in standard versus indicated amino acid-starved media. Results shown as $\log_2$ fold change of area under curve (AUC) normalized to average standard media. Each column for each condition represents a technical replicate (n=5/condition). Gray indicates that given condition is lethal.

(D) Distribution of AUC and IC_{50} for human AML cell lines with OTX015 for 5 days. Error bars represent mean ± SD of seven technical replicates.

(E) Distribution of IC_{50} for human AML cell lines with JQ1 (left) or THZ1 (right) for 5 days. Error bars represent mean ± SD of five technical replicates.

(D-E) * p value ≤ 0.05 versus + folic acid condition calculated with Mann-Whitney test.

(F) Two human AML cell lines were infected with two *BRD4*-directed shRNAs and grown in regular versus folic acid-starved media. Growth after treatment with 0.5μg/ml doxycycline normalized to control and shown relative to day 0 (time of seeding). Error bars represent mean ± SD of five technical replicates. * p value ≤ 0.05 calculated with Welch's t-test versus shCT.

(G) Colony formation from human U937 AML cells with 300nM OTX015 and indicated folic acid concentrations. Results represent average of triplicate assays. *p-value ≤ 0.05 calculated with Welch's t-test versus 1mg/L folic acid condition. Error bars represent mean ± SD.

(H) Bar graphs showing proportion of U937 and MOLM-14 human AML cells in apoptosis (Annexin $V=A^+$/propidium iodide=PI^+) with 750nM OTX015 combined with folic acid restriction. *p-value ≤ 0.05 with Welch's t-test versus OTX015-treated cells grown in folic acid. Error bars represent mean ± SD of three technical replicates.

(I) Distribution of IC_{50} for four *MLL*-translocated AML patient samples with OTX015 for 5 days. p-value calculated using nonparametric Mann-Whitney test. Error bars represent mean ± SD.

(J-K) Mice fed regular or folic acid-restricted diet one month before injection of murine Ds-Redpositive MLL-AF9-driven leukemic cells. Mice treated with either vehicle or 35 mg/kg JQ1 for 7 days. Assessment of plasma homocysteine and methionine levels **(J)**, and flow cytometry-based quantification of Ds-Red-positive leukemic blasts in bone marrow **(K)**. p-value calculated using nonparametric Mann-Whitney test. n.s, nonsignificant (p > 0.05). Error bars represent mean ± SD of four mice/group.

Each experiment in C–H performed at least twice.

Each experiment in C–H performed by comparison of standard media (1000 ng/mL folic acid) and no folic acid media (0 ng/mL folic acid).

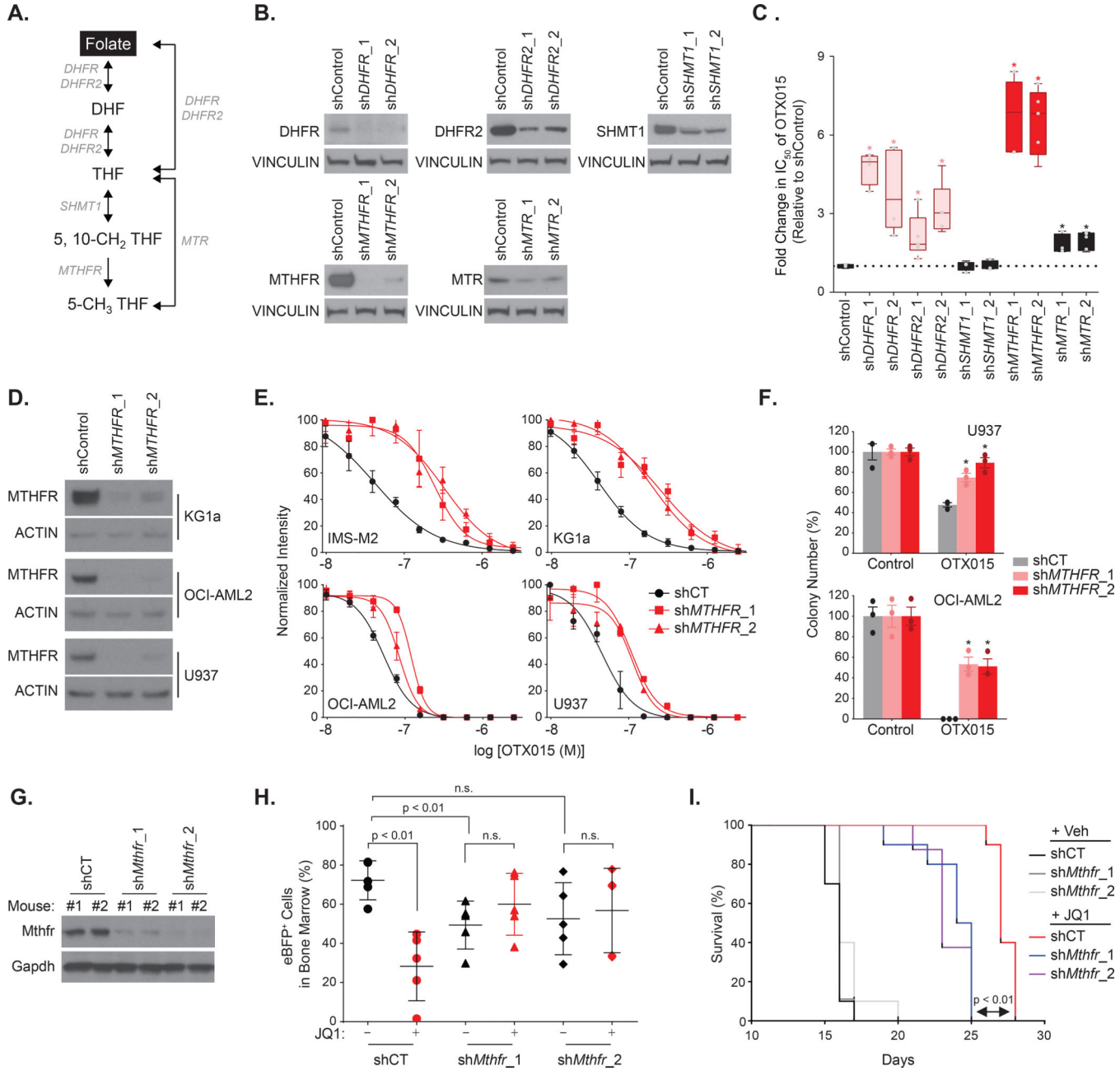

Figure 2: MTHFR suppression enhances resistance to BET inhibitors.

(A) Schematic of folate cycle, involved enzymes.

(B) Immunoblot for each indicated enzyme, and VINCULIN (loading control) from human IMS-M2 cell line infected with control or two shRNAs.

(C) Fold change in IC_{50} of OTX015 in IMS-M2 cells infected with indicated shRNAs targeting folate cycle enzymes. Results shown as fold change of IC_{50} normalized to average shControl. *p-value ≤ 0.05 by nonparametric Mann-Whitney test. Error bars represent mean ± SD of four technical replicates. Experiment performed at least two independent times.

(D) Immunoblot for MTHFR and VINCULIN (loading control) from indicated human AML cell lines infected with control or two *MTHFR*-directed shRNAs (sh*MTHFR*_1 and sh*MTHFR*_2).

(E) Growth inhibition of indicated AML cell lines infected with control or two *MTHFR*-directed shRNAs (sh*MTHFR*_1 and sh*MTHFR*_2) and treated with increasing OTX015 for 5 days. Error bars represent mean ± SD of seven technical replicates.

(F) Colony formation from human U937 and OCI-AML2 AML cells infected with control (shCT) or *MTHFR*-directed shRNAs, and treated with 100nM and 30nM OTX015, respectively. Results represent average of triplicate assays. *p-value ≤ 0.05 by Welch's t-test versus shCT. Error bars represent mean ± SD.

Each experiment in E and F performed at least two independent times.

(G) Immunoblot for Mthfr knockdown in murine eBFP-sorted bone marrow MLL-AF9-driven leukemic cells. Two mice depicted per condition.

(H) Proportion of eBFP-positive MLL-AF9 leukemic cells harboring control (shCT) or two *Mthfr*-directed shRNAs (sh*Mthfr*_1 and sh*Mthfr*_2) in bone marrow from five mice per group treated with vehicle or 35mg/kg JQ1 for 7 days. p-value ≤ 0.01 by Mann-Whitney test. n.s, nonsignificant (p > 0.05). Error bars represent mean ± SD.

(I) Kaplan-Meier curves showing overall survival of mice (n = 5 for each group) transplanted with MLL-AF9-positive blasts infected with control (shCT) or two *Mthfr*-directed shRNAs and treated with vehicle or 35mg/kg JQ1 for 7 days. Statistical significance by log-rank (Mantel-Cox) test.

Each experiment in H and I performed at least two independent times.

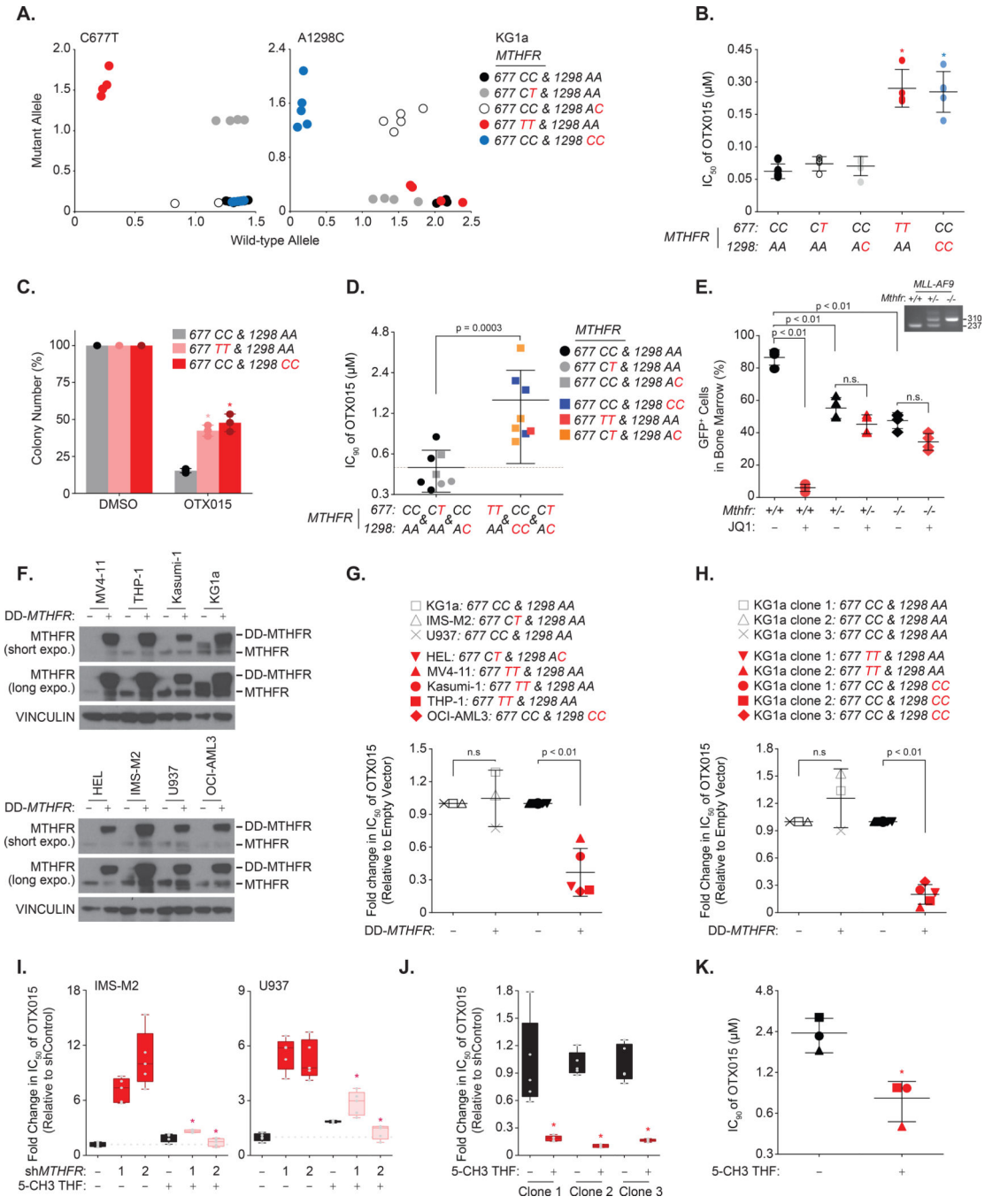

Figure 3: *C677T* and *A1298C MTHFR* variants promote resistance to BET Inhibitors.

(A) Allelic discrimination plots depicting polymorphic status of *MTHFR* at C677 and A1298. Five CRISPR/Cas9-edited KG1a clones with various *MTHFR* genetic variants on C677 and A1298 were selected.

(B) Distribution of IC_{50} with OTX015 for 6 days of CRISPR/Cas9-edited KG1a clones exhibiting various *MTHFR* genetic variants (n=5 clones per genotype). *p-value ≤ 0.05 by nonparametric Mann-Whitney test. Error bars represent mean ± SD. Experiment performed at least two independent times.

(C) Colony formation from CRISPR/Cas9-edited KG1a clones exhibiting various *MTHFR* genetic variants with 1μM OTX015. Results represent average of triplicate assays. *p-value ≤ 0.05 by Welch's t-test versus MTHFR 677CC & A1298AA clone with OTX015. Error bars represent mean ± SD.

(D) Distribution of IC_{90} with OTX015 for 5 days of 16 *MLL*-translocated patient samples with AML divided into 2 subgroups according to MTHFR genetic status at C677, A1298. p-value by nonparametric Mann-Whitney test. Error bars represent mean ± SD.

(E) MLL-AF9-transformed GFP-positive granulomonocytic progenitors (Sca-1^-/c-KIT^+/$CD16/32^+$/$CD34^+$/MPO^+) from homozygous wild-type (+/+), or heterozygous (+/−) and homozygous (−/−) *Mthfr* knockout mice transplanted into sublethally-irradiated recipient mice before treatment with vehicle or 50mg/kg JQ1 for 7 days. Proportion of GFP-positive MLL-AF9 leukemic cells in bone marrow from five mice per group. p-value by Mann-Whitney test. n.s, nonsignificant ($p > 0.05$). Error bars represent mean ± SD.

(F) Immunoblot for MTHFR and VINCULIN (loading control) from human AML cell lines overexpressing wild-type DD-tagged MTHFR.

(G-H) Fold change in IC_{50} of OTX015 for 5 days in AML cell lines **(G)** or CRISPR/Cas9-edited KG1a clones **(H)** expressing a construct encoding either empty control or DD-tagged wild-type *MTHFR* divided into two groups according to *MTHFR* genotypes at C677, A1298. Results shown as fold change of IC_{50} normalized to average empty vector condition. *p-value by nonparametric Mann-Whitney test. n.s, nonsignificant ($p > 0.05$). Error bars represent mean ± SD.

(I-J) Fold change in IC_{50} of OTX015 in IMS-M2 and U937 cells infected with control or two *MTHFR*-directed shRNAs **(I)** or indicated CRISPR/Cas9-edited KG1a clones **(J)** with 50μM 5-CH_3 THF for 5 days. Results shown as fold change of IC_{50} normalized to average untreated condition. *p-value ≤ 0.05 by nonparametric Mann-Whitney test. n.s, nonsignificant ($p > 0.05$).

Error bars represent mean ± SD.

Each experiment in G–J performed at least two independent times.

(K) Distribution of IC_{90} to OTX015 for 5 days and 50μM 5-CH_3 THF treatment of three *MLL*-translocated AML patient samples. Square represents a patient with *MTHFR* 677 CT & 1298 AC genotype; the two others exhibit *MTHFR* 677 CC & A1298 CC genotype. *p-value ≤ 0.05 by nonparametric Mann-Whitney test. Error bars represent mean ± SD.

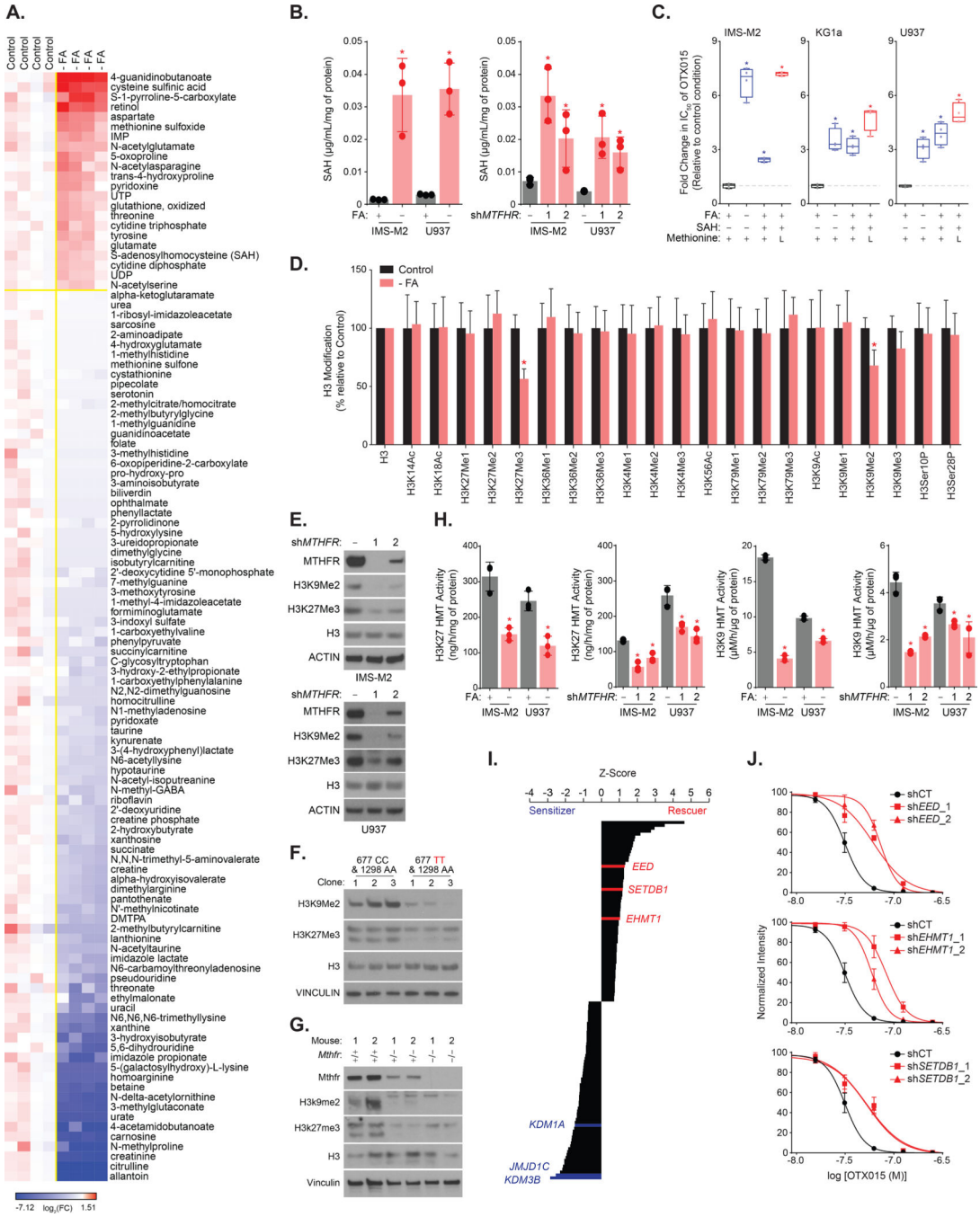

Figure 4: Folate cycle disruption impacts metabolic and histone H3 methylation state in AML cells.

(A) Heatmap of top upregulated or downregulated metabolites (p-value ≤ 0.05) identified by steady-state metabolism profiling in human U937 cells in standard or folic acid-restricted media (− FA). Each column for each condition represents a technical replicate (n=4 per condition).

(B) Intracellular SAH in indicated human AML cell lines with folic acid (FA) withdrawal (leftl) or MTHFR suppression using two MTHFR-directed shRNAs (shMTHFR_1 and

shMTHFR_2, right). *p-value ≤ 0.05 by Welch's t-test versus respective control. Error bars represent mean ± SD of three technical replicates.

(C) Fold change in IC_{50} of OTX015 for 5 days in human AML cell lines depleted or supplemented with indicated metabolites. L = low. Results shown as fold change of IC_{50} normalized to average control condition. SAH was used at 50μM. *p-value ≤ 0.05 by nonparametric Mann-Whitney test. n.s, nonsignificant (p > 0.05). Error bars represent mean ± SD of five technical replicates.

Each experiment in A–C performed at least two independent times.

(D) ELISA quantification of H3 modifications with folic acid withdrawal in U937 and IMS-M2 AML cells. Results normalized to total H3 per cell type and shown relative to average control across the two lines. *p-value ≤ 0.05 by nonparametric Mann-Whitney test. Error bars represent mean ± SD of three technical replicates per line.

(E-G) Immunoblot for MTHFR, H3K9Me2, H3K27me3, total H3, ACTIN, and VINCULIN (loading control) from indicated human AML cell lines (E), CRISPR/Cas9-edited KG1a clones exhibiting indicated *MTHFR* genetic variants (F), and primary MLL-AF9-expressing bone marrow either wild-type (+/+), or heterozygous (+/−) and homozygous (−/−) *Mthfr* knockout murine cells (G).

(H) Quantification of H3K27me3 (right) and H3K9Me2 (left) methyltransferase activities in U937 and IMS-M2 cells upon folate withdrawal or MTHFR knockdown (shMTHFR_1 and shMTHFR_2). *p-value ≤ 0.05 by Welch's t-test versus respective control. Error bars represent mean ± SD of three technical replicates.

(I) Waterfall plot of top rescuers of or sensitizers to JQ1 from CRISPR/Cas9-based screen on epigenetic regulators. Absolute cut-off of z-score ≥ 0.70 defines rescuers and z-score ≤ −0.70 defines sensitizers. In red and blue are H3K27me3 or H3K9me2 methyltransferases and demethylases, respectively.

(J) Growth inhibition of U937 cells expressing control hairpin (shCT) or hairpins against *EED*, *EHMT1*, or SETDB1 and treated with increasing OTX015 for 6 days. Error bars represent mean ± SD of seven technical replicates. Experiment performed at least two independent times.

Each experiment in B–D, and H performed by comparison of standard media (1000 ng/mL folic acid) and no folic acid media (0 ng/mL folic acid).

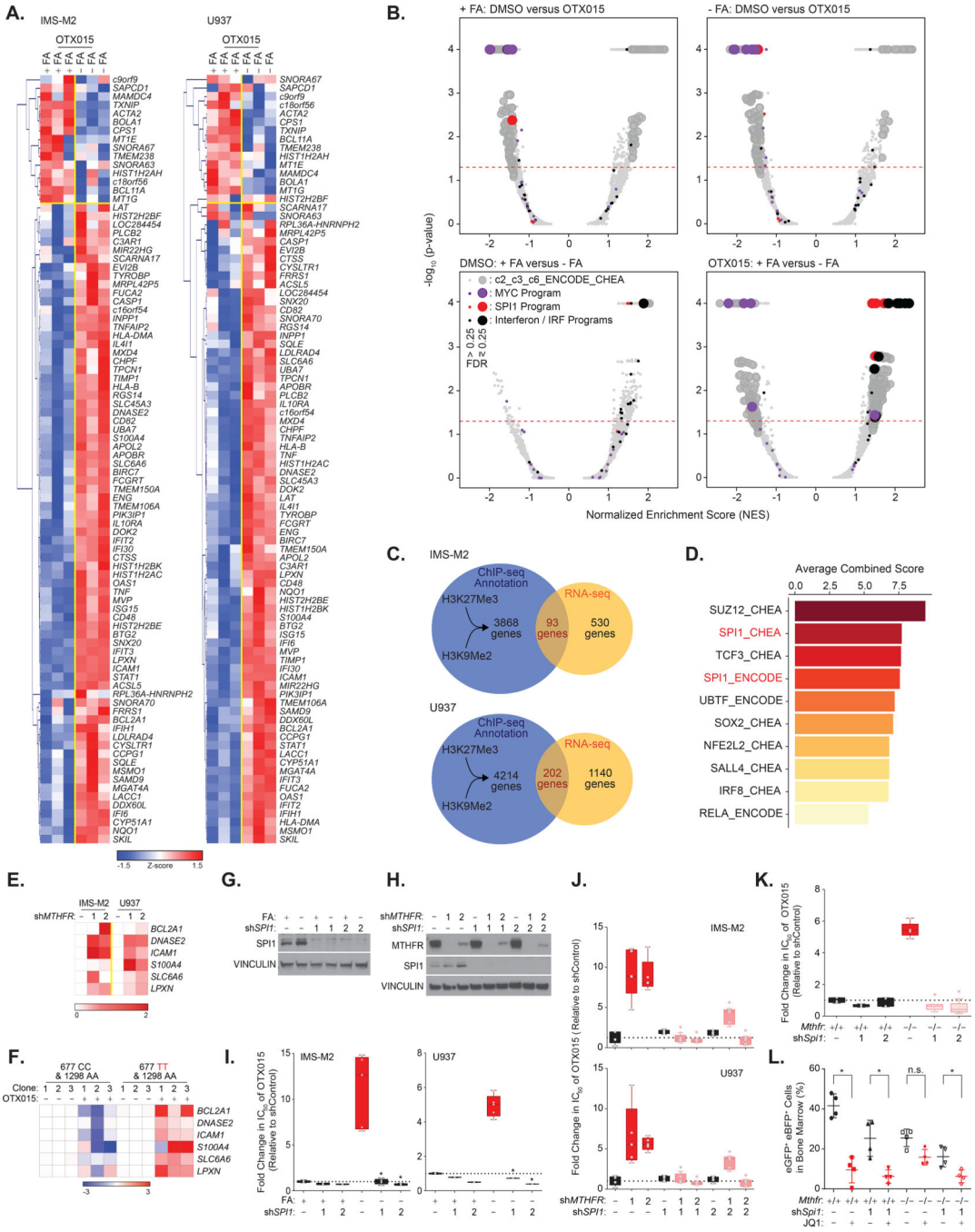

Figure 5: Folate cycle disruption combined with BET inhibitors activate a SPI1 transcriptional program.

(A) Heatmap of top common up- and down-regulated genes in human IMS-M2 and U937 cell lines with 1μM and 300nM OTX015, respectively for 24 hours in regular (1000 ng/mL folic acid) versus folic acid-deprived media (0 ng/mL folic acid). p-value ≤ 0.05, FDR ≤ 0.05, and absolute fold change for log2(FPKM) scores ≥ 1.5. Each column for each condition represents an independent biological replicate (n=3 per condition in two human cell lines).

(B) Quantitative comparison of gene sets from MSigDB, ENCODE, and CHEA by GSEA for IMS-M2 and U937 cell lines. Top volcano plots compare DMSO versus OTX015 in +folic acid (+FA) or -folic acid (−FA) conditions. Bottom volcano plots compare +FA versus −FA in DMSO- or OTX015-treated cells. Red indicates sets for *SPI1* program, black for Interferon / *IRF* program, purple for *MYC* program, and gray for all other available gene sets. All datasets above dashed red line have p-value ≤ 0.05, big dots have FDR ≤ 0.25.
(C) Venn diagrams for integrative analysis deployed to select top genes from ChIP-Sequencing and RNA-sequencing in IMS-M2 and U937 cells.
(D) Enrichr overlapping analysis of top-enriched transcription factor-related gene sets from combined list of genes identified at intersection of ChIP- and RNA-sequencing in IMS-M2 and U937 cell lines.
(E-F) Heatmap showing expression of SPI1 transcriptional targets by qRT-PCR. Normalized data presented as log2-ratio versus control shRNA (shCT) **(E)** or log2-ratio versus DMSO-treated clones **(F).** Experiment performed at least two independent times.
(G-H) Immunoblot for MTHFR, SPI1, and VINCULIN (loading control) from U937 cells infected with control or two *SPI1*-directed shRNAs (sh*SPI1*_1 and sh*SPI1*_2) with folic acid (FA) withdrawal **(G)** or in combination with MTHFR depletion using *MTHFR*-directed shRNAs (sh*MTHFR*_1 and sh*MTHFR*_2) **(H).**
(I-J) Fold change in IC_{50} of OTX015 for 5 days in U937 and IMS-M2 cells infected with control or two *SPI1*-directed shRNAs and starved from folic acid (−FA, 0 ng/mL folic acid) **(I)** or co-infected with control or two *MTHFR*-directed shRNAs **(J)**.
(K) Fold change in IC_{50} of OTX015 for 5 days in homozygous wild-type (+/+) or homozygous (−/−) *Mthfr* knockout MLL-AF9 leukemic cells infected with control or two *Spi1*-directed shRNAs.
(I-K) Results shown as fold change of IC_{50} normalized to average shControl. *p-value ≤ 0.05 by nonparametric Mann-Whitney test. n.s, nonsignificant (p > 0.05). Error bars represent mean ± SD of five technical replicates.
Each experiment in E, F, and I–K performed at least two independent times.
(L) Proportion of eGFP- and eBFP-positive expressing either a control (shCT) or a *Spi1*-directed shRNA (sh*Spi1*_1) in bone marrow from four mice per group treated with either vehicle or 50mg/kg JQ1 for 7 days. *p-value ≤ 0.05 by Mann-Whitney test. n.s, nonsignificant (p > 0.05).
Error bars represent mean ± SD.